THE JOURNAL OF PHYSICAL CHEMISTRY B

Article

pubs.acs.org/JPCB

Free Energy of Separation of Structure II Clathrate Hydrate in Water and a Light Oil

Bjørn Steen Sæthre,[†] David van der Spoel,[‡] and Alex C. Hoffmann*[,†]

[†]Department of Physics and Technology, University of Bergen, Allegaten 55, 5007 Bergen, Norway

[‡]Department of Cell and Molecular Biology, Uppsala University, Husargatan 3, Box 596, SE-75124 Uppsala, Sweden

ABSTRACT: The adhesion forces and free energies of separation of structure II clathrate hydrates in vacuum and submerged in water and a model oil are investigated by molecular dynamics simulation. The water molecules are modeled by the TIP4P/ice model and the alkanes by the OPLS_AA force field. The results are compared with theory and earlier work. It is observed that the adhesive forces between the simulated surfaces have an effective range of no more than 1.5−2 nm. The hydrate−hydrate interaction force is attractive in vacuum and oil, larger in vacuum. In water the interaction force is very slightly repulsive on average and much weaker than in the two other systems with a larger uncertainty. In all cases the interaction is largely entropically driven. The separation energies in vacuum and oil (octane) are stronger than predicted by theory, with free energies of approximately 4 and 0.7 aJ, respectively, likely due to lack of polarization effects. The hydrate−hydrate interaction in water is too weak for quantitative comparisons to be made.

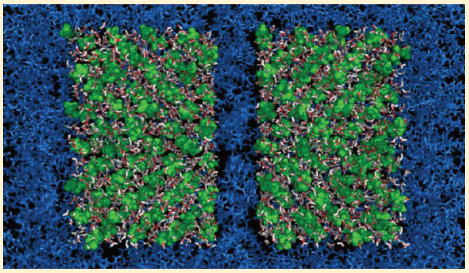

INTRODUCTION

Gas hydrates are crystalline compounds consisting of water molecules encaging gas molecules.[1] They are found mainly in two types of structures, structure I and II, depending upon the size of the included gas molecules and the composition of their mixture. The hydrates are stable at elevated pressures, even above the normal melting point of ice.[2,3] Hydrate formations are thus abundant on/near the sea floor but also in land areas with arctic permafrost.[4−6] Gas hydrates were, however, first discovered in production pipelines, where they present a continuing challenge for flow assurance.[7] The problem of hydrate plugs is normally mitigated by thermodynamic inhibition, typically involving adding large quantities of defrosters, like methanol or glycols, to production lines.[8] However, increasingly kinetic inhibitors and antiagglomerants are replacing this due to considerations of cost-effectiveness and environmental friendliness.[9,10]

It is known that hydrate wettability is a crucial factor in the tendency of hydrate particles to form plugs.[11,12] It can be expected that the interactions between the hydrate surface and the surrounding fluid medium plays a major role in determining the extent of wetting.[13,14]

The focus of this study is to explore whether the interaction between hydrate particles can usefully be modeled by direct molecular dynamics simulations. If this is the case, molecular dynamics models may be used to determine the effect of the nature of the carrier fluid(s), and specifically of various species present in the carrier fluids, on the cohesivity of hydrate particles. This, in turn, may point the way to mitigating the buildup of hydrate plugs in pipelines by the addition of deagglomerants to the pipeline fluids containing the particles.

An additional argument for exploring the usefulness of molecular dynamics models is that it has been difficult to determine surface and interface energy for hydrates by experiment,[15] although observations of growth regimes[16] hint to its importance. In this work a direct approach is taken by seeking to determine the free energy of separation of hydrate slabs in model fluids of oil and water through molecular dynamics simulations. This involves simulating direct force measurements[17] between hydrate slabs,[18] albeit on the nanometer scale.

A recent study by Mastny et al. focuses on the effect of the water/methane interface on hydrate energetics.[19] Mastny et al. studied the melting of hydrate cages and the forces acting between individual cages. The present authors have previously studied liquid mixtures between quartz plates[20] and computed the potential of mean force (PMF) of pulling apart the plates, thereby creating a vacuum. In this present work the hydrate crystals are completely immersed in light oil or water, and it therefore represents a somewhat different problem. The energies are therefore expected to be lower.

THEORY

The following five contributions may be taken into account when determining the molecular interactions in hydrate/fluid systems:[21] (1) the hydrogen bond, which, within its very short range, can be described as a charge−dipole interaction;[21] (2) the directional dipole−dipole interaction between fixed dipoles in the hydrate crystal; (3) the directionally averaged dipole−dipole interactions arising from the dipoles in the fluid that are free to rotate; (4) the dipole−induced dipole interactions; (5) the induced dipole−induced dipole dispersion interactions.

Received: January 8, 2012
Revised: April 18, 2012
Published: April 27, 2012

dx.doi.org/10.1021/jp300230p | J. Phys. Chem. B 2012, 116, 5933−5940

Together, these forces result in a molecular interaction potential of the form

$$u_{\mathrm{mol}}(r) = -C_{\mathrm{vdw}}/r^6 - \sum_i [C_{\mathrm{dip}}(\Omega_i, \vec{\mu}_i)/r^3 + C_{\mathrm{hb}}(\Omega_i, \vec{\mu}_{wi})/r^2] \quad (1)$$

where r is the intermolecular distance, C_{vdw}, C_{dip}, and C_{hb} are constants describing the van der Waals, fixed dipole, and hydrogen bond interactions, respectively, $\vec{\mu}$ is the dipole strength and orientation, and Ω indicates the dependency on the angles of the dipoles. It is understood that the last term under the summation sign is only valid within the very short-range of the hydrogen bond. C_{vdw} is given by

$$C_{\mathrm{vdw}} = \frac{1}{(4\pi\varepsilon_0)^2}\left(\frac{(\mu_1\mu_2)^2}{3kT} + (\alpha_1{\mu_2}^2 + \alpha_2{\mu_1}^2) + \frac{3\alpha_1\alpha_2\hbar\omega_1\omega_2}{2(\omega_1+\omega_2)}\right) \quad (2)$$

the three terms involving C_{vdw} corresponding to effects 3−5 above and constituting the van der Waals forces. In this equation μ are the dipole moments, α are the polarizabilities, and k, T, ε_0, $\hbar$, and ω have their usual meanings. C_{dip} and C_{hb} depend on individual molecular orientations in addition to material properties, and the sum is taken over all other molecules in the system.

In crystals studied at large enough scales, the total net dipole moment is close to zero, since otherwise the material would quickly become mechanically unstable. In the nanoscale systems in this present work efforts have been made to prepare the systems with minimal total dipole moments, so as to minimize the influence of the directional dipole term on the hydrate/fluid interactions.

Hydrogen bonds constitute the major interaction stabilizing the hydrate crystal, and hydrogen-bonding effects are likely to play some role in the energy of separation in the present systems. This would be strongest in the hydrate/vacuum case; when liquid water is present, hydrogen-bonding effects should become more short-ranged.

Taking into account that problems with total dipole moments have been minimized (see below) and effects of hydrogent bonds are rather short-ranged, and to simplify modeling, the dipole interactions under the summation sign in (1) that cannot be angle-averaged, and are therefore directional, are ignored in what follows.

Integrating the short-range part of (1) up for a planar geometry[21] then yields an attractive force term of the form $F_{\mathrm{ad}} \propto -1/r^3$.

As will be shown later, simulation results for the hydrate/vacuum system indicated that also a repulsive force can be identified when the separation between the hydrate slabs is very small (see (4) later in the paper). To achieve a decent fit to these results, a repulsive force term is therefore also required in the hydrate/vacuum case, thus ending up with an integrated force function of the form

$$P(r) = \frac{F(r)}{A_c} = \frac{A}{r^9} - \frac{B}{r^3} \quad (3)$$

where A_c is the area of the hydrate surface on the pulled hydrate slab facing the reference slab.

DLP Theory. The Dzyaloshinski−Lifshitz−Pitaevki (DLP) theory[22] offers an approximate treatment of quantum-mechanical (QM) many-body interactions, based on a macroscopic continuum theory, starting from the general dielectric response function, ε, as the fundamental material property. This response function can be related to more familiar properties as

$$\varepsilon(\omega) = (n(\omega) + ik(\omega))^2 \quad (4)$$

where $n(\omega)$ is the frequency-dependent index of refraction function and k is the absorption spectrum of the medium. The theory is presented in a hybridized QM-classical form by Bonnefoy et al.[23] Applying their treatment to structure II propane hydrate makes it possible to compare the simulation results in this work with theoretical expectations.

According to this model, the interaction potential between two macroscopic bodies, 1 and 2, separated by a distance D with intervening fluid 3 is

$$V(D) = -A_{132} f_{D,\mathrm{geometry}} \quad (5)$$

The Hamaker−Lifshitz factor A_{132} depends on geometry (it is invalid for nonsmooth surfaces, for example), thermodynamic state, and material properties and can be expressed as

$$A_{132} = \frac{3kT}{2}\sum_{n=0'}^{\infty}\sum_{m=1}^{\infty}\left(\frac{\varepsilon_1(i\omega_n) - \varepsilon_3(i\omega_n)}{\varepsilon_1(i\omega_n) + \varepsilon_3(i\omega_n)}\frac{\varepsilon_2(i\omega_n) - \varepsilon_3(i\omega_n)}{\varepsilon_2(i\omega_n) + \varepsilon_3(i\omega_n)}\right)^m m^{-3} \quad (6)$$

with $\hbar\omega_n/kT = n$, $n = 1, 2, \ldots$.

f is a geometric factor. For planar slabs f is given by[21]

$$f = \frac{1}{12\pi}\left(\frac{1}{D^2} + \frac{1}{(D+2L)^2} - \frac{2}{(L+D)^2}\right) \quad (7)$$

for the planar dimension L.

Free Energy Difference of Separation from Constraint-Force Simulations. The potential of mean force is equal to the free energy difference of two states expressed in terms of some geometrical parameter. In this study the free energy is determined as a function of the normal separation, z, sampling from a canonical ensemble.[24]

$$\mathcal{F} - \mathcal{F}_0 = \int_{Z_0}^{Z_{\max}} \left\langle \frac{\partial H}{\partial z} \right\rangle_z \mathrm{d}z \quad (8)$$

Here $\mathcal{F}$ is the Helmholz free energy of separation, H is the Hamiltonian, and $\langle\ \rangle_z$ denotes the trajectory average at constant separation, z, assuming the system to be ergodic.

There are several methods applicable for estimating $\langle \partial H/\partial z \rangle$. For a separation process as the present, where two surfaces are pulled apart, simulations wherein the surface separation is constrained are the obvious choice. Then the force needed to enforce the constraint on the separation can be identified as $\langle f_c(z) \rangle = \langle \partial H/\partial z \rangle$. Inserting this into eq 8 yields

$$\mathcal{F} - \mathcal{F}_0 = \int_{Z_0}^{Z_{\max}} \langle f_c(z) \rangle \, \mathrm{d}z \quad (9)$$

where the reference is chosen as a particular surface separation. The adhesive force between the two slabs is the reaction force of the imposed constraint force.

This integral can be estimated by sampling a few points of the constraint force along a path separating the two states. The integration is done numerically by cubic interpolation. Assuming that uncertainties in $\langle f_c(z) \rangle$ for different z values are uncorrelated, the Euclidean norm can be used for estimating error propagation.

The internal energy $\mathcal{U} = \langle E_{\mathrm{tot}} \rangle$, and the entropy can therefore be obtained from the difference $T\mathcal{L} = \mathcal{U} - \mathcal{F}$. In actual

dx.doi.org/10.1021/jp300230p | J. Phys. Chem. B 2012, 116, 5933−5940

calculations the same reference is chosen for all the state functions.

METHODS

Interaction Potential and Molecular Models. The OPLS-AA force field[25] is employed for the organic compounds and the rigid TIP4P/ice[26] model for the water molecules. The pairwise intermolecular potential contains both Lennard-Jones (LJ) terms for the van der Waals-type interactions and pure Coloumbic terms to model the polar character of the water molecule:

$$U = \sum_{i>j} \left(4\varepsilon_{ij} \left(\left(\frac{\sigma_{ij}}{r_{ij}} \right)^{12} - \left(\frac{\sigma_{ij}}{r_{ij}} \right)^{6} \right) + \frac{q_i q_j}{4\pi r_{ij}} \right) \quad (10)$$

where ε_{ij} and σ_{ij} are the usual Lennard-Jones parameters. All water molecules are constrained to be fully rigid by the SETTLE algorithm.[27] The oil is modeled as pure 1-octane, and the guest molecules in the structure II hydrates are assumed to be propane molecules occupying the large $5^{12}6^4$ cages only. The propanes and octane molecules have intramolecular bond lengths constrained using the P-LINCS[28] algorithm.

System Design. The construction of the structure II hydrate from the unit cell (UC) is described below.

The component molecules were built from scratch, using the software Arguslab[29] and the PRODRG server.[30] An initial energy minimization on each molecule was done using the semi-empirical Quantum-Hamiltonian AM1[29] implemented in the ArgusLab program to force the molecules to a realistic starting geometry.

The GROMACS suite[31] was used for modeling and analysis, and Grace and VMD[32] were used for data presentation and trajectory visualization. The OPLS-AA-force field of Jorgensen et al.[33] was used to model the organic molecules and the compatible TIP4P[34] model for the water molecules.

The pure-component phases were set up by creating and randomly inserting component molecules in cubic or slightly rectangular boxes. The size of these boxes were set so that the initial material densities agreed roughly with the physical densities of the materials.

The structure II propane–hydrate crystal was prepared in five steps:

1 *Water framework.* The hydrate crystal unit-cell oxygen positions were constructed from the asymmetric unit obtained from McMullan and Jeffrey[35] using the space group symmetry transformations of *Fd*3*m*, input into a unit cell with tentative lattice vectors a = 1.72 nm.[36]

   TIP4P waters were constructed, based on the above oxygen positions, and the system then subjected to steepest descent energy minimization with periodic boundary conditions, and subtraction of the translational center-of-mass-movement, to allow natural alignment of hydrogen along the cage edges. After inspection of the trajectory it was not deemed necessary to fix the oxygens during this process as their dominant total mass, together with the periodicity of the system and the center-of-mass-motion removal, made for a negligible oxygen displacement.

2 *Guest insertion.* The earlier prepared single propane guest molecules were copied and positioned into all the vacant large cages in the unit cell. The middle C atom in each propane was used as a center-of-mass estimate and aligned with the cage centers.

3 *Energy minimization of unit cell.* A steepest gradient method was used, moving the guests into their exact centers in the cages by removing the stretch introduced into the propanes in the insertion step and rotating them into their lowest energy position.

4 *Hydrate system assembly.* A hydrate structure was then constructed by creating a template of 3 × 3 × 2 unit cells in a 3 × 2 × 4 UC structure of side lengths 5.1 × 3.4 × 3.4 nm.

5 *Energy minimization of template.* It was necessary to do a final energy minimization on the total system, during which the carbon backbones of the guests were restrained by employing a large harmonic force with spring constant k = 10 000 kJ (mol nm^2)$^{-1}$ to prevent strange guest molecule deformations. For the same reason the number of steps of energy minimization was made relatively small, but sufficient to observe an almost complete flattening of the potential energy curve. The reason for the necessity of this step is likely an edge effect (i.e., guest molecules being partly outside cages in the unit cell energy minimization step).

The general geometry of the system is shown in Figure 1. The hydrate slab geometry is created by stacking together unit cells in two 3 × 2 × 2 UC blocks. The gap is created along the z-coordinate direction by pure translation. That is, the slabs would, if brought back into contact, form a rectangular block of 3 × 2 × 4 UCs. The face exposed is the (100) Miller plane, which was the most convenient from a practical point of view. Exposing other planes may have an effect on the results.

The hydrate slabs are equilibrated, and the internal dipoles randomized by a simulated annealing procedure detailed below. The fluids are equilibrated at the same temperature and at a pressure of about $P \sim 10$ bar.

The geometrical configurations simulated are then created by displacing the slabs along the reaction coordinate to form a set of 20 separations for each hydrate/fluid combination and then adding vacuum on the external surfaces. The box dimensions in these final configurations are 8 × 6 × 12 nm. The step size in separations was thus 0.1 nm, which was the smallest step size for which we perceived significant changes in the system. The temperature was 254 K, this to ensure the stability of the crystals during the relatively long simulation time while maintaining propane in the gaseous form. In the systems involving water, which was prepared as "bricks" (see below) at 280 K before insertion into the computational box, this means that the liquid phase can only be considered pseudostable.

The submerging fluid is then added in the available vacuum, first by stacking together rectangular "bricks" of fluid and thereafter by randomly placing fluid molecules into the remaining space available, their position constrained by the van der Waals radii of the surrounding atoms.

The resulting system size varied between 50 000 and 90 000 atoms in total, with the higher numbers occurring for the hydrate/water systems. The ensuing total system was thoroughly equilibrated for 100–200 ps before data collection.

Simulation Parameters. The simulations were performed using the GROMACS engine.[31,37] Constant volume, temperature, and particle number confined the systems to the canonical ensemble. A total of 4 ns was simulated for each hydrate/water simulation. In the hydrate/vacuum and hydrate/oil systems 2 ns

dx.doi.org/10.1021/jp300230p | J. Phys. Chem. B 2012, 116, 5933–5940

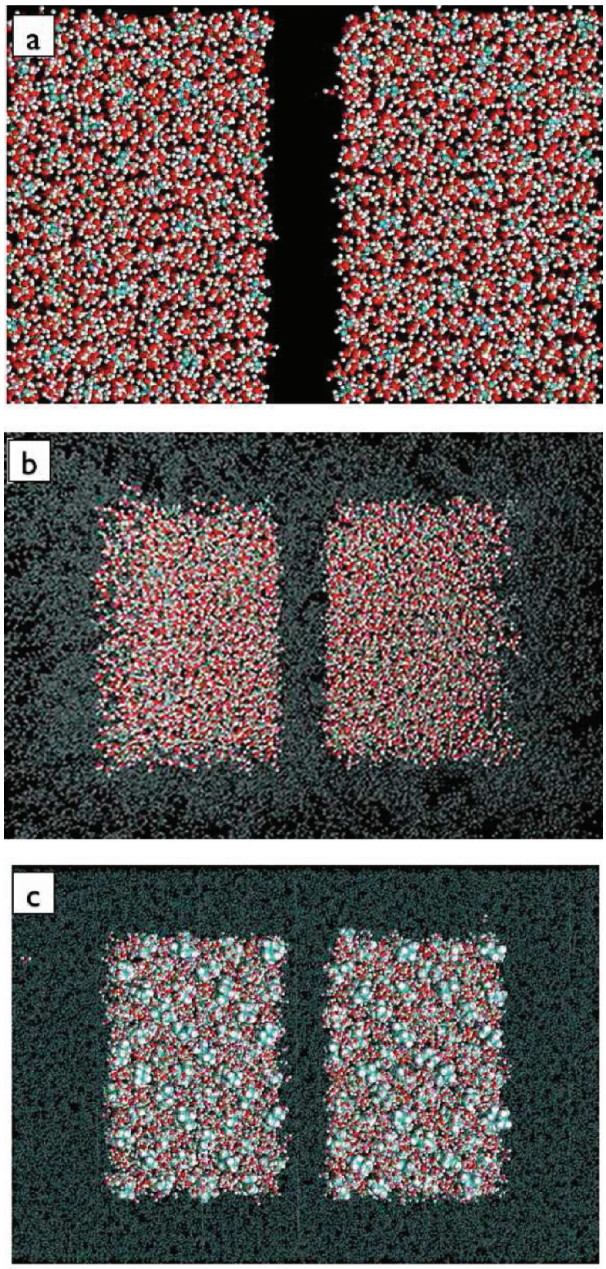

Figure 1. Simulation setup for class II hydrates (a) in vacuum, (b) in oil (the long oil molecules have not been "wrapped" back into the computational box), and (c) in water.

simulations were deemed sufficient. A step size of 2 fs was used in each simulation, as the only intramolecular degree of freedom was the CCC angle vibrations.[38]

Neighbor searching was performed every five steps. The particle mesh Ewald algorithm[39] was used for electrostatic interactions with a cutoff of 0.9 nm. A reciprocal grid of 64 × 48 × 96 cells was used for the particle mesh, corresponding to a direct-space cutoff of 0.125 nm. Sixth-order B-spline interpolation was used in the method. A single cutoff of 0.9 nm was used for van der Waals interactions. Temperature coupling was done with the Berendsen algorithm.[40] A Lennard-Jones dispersion correction for the cutoff was applied to both the energies and the pressure.[38]

The constraint force pulling was imposed by the use of the analytical SHAKE[41] algorithm with two groups, the pull group being the top hydrate slab (1) the reference group being the lower one. The constraint force was updated every step. The pulling was constant-directional along the initial separation vector between the slab centers of mass. The tolerance of the constraint was $d_{tol} = 10^{-4}$ nm.

Global Energy Minimization by Simulated Annealing. The hydrate structure II in bulk is well-known to be a proton-disordered lattice structure with zero total dipole moment conforming to the Bernal–Fowler ice rules.[42,43] Ice Ih, and by analogy likely hydrate, shows increased ordering toward external surfaces.[44] Gauging the present system, the net total dipole moment for 1632 water molecules was found to be 600 D, which suggested an initial artificial ordering of the moments. That is, the aforementioned energy minimization did not succeed in finding the global energy minimum of the hydrate crystal.

Simulated annealing is a well-known procedure, based on the observation that slow cooling of molten metal allows the metal to reach its crystalline, lowest-energy configuration as opposed to e.g. an amorphous solid form. A similar method is used in molecular modeling to find the global energy minimum of a system or a global minimum of some fitness function in a general optimization problem; see for instance ref 45. The method avoids being trapped in a local energy minimum by allowing "uphill" steps ΔE with probability $P \propto \exp(-\Delta E/k_B T)$, only restricting the search space at lower temperature, similar to a Monte Carlo scheme.

The removal of most of the net dipole moment was achieved by: *Breaking H-bonds*: scaling up the hydrate isotropically to break the hydrogen bonds. *Heating up*: constraining the oxygen to fixed positions and heating up the structure well past boiling point ("frozen vapor"). *Annealing*: performing a simulated annealing: A slow cooling with pressure control while keeping the relative oxygen coordinates fixed.

RESULTS AND DISCUSSION

Annealing. The time development of the simulated annealing procedure is plotted in Figure 2. Annealing reduces μ_{tot} in the simulation box from $\mu_{tot} \sim 600$ D to $\mu_{tot} \sim 50$ D. This can be compared to the dipole moment per water molecule $\mu_{mol} = 2.43 \pm 0.02$ D at $T = 250$ K.

Despite being significantly lower, a residual ordering can be seen still to be present. For this geometry the initial $\mu_y \approx 200$ D corresponds to 5% of the molecules having their dipoles aligned along the y coordinate. The infinite-system Kirkwood factor,[46] defined as

$$g_k = \frac{2\varepsilon + 1}{3\varepsilon} \frac{\langle M^2 \rangle}{N_p \langle \mu^2 \rangle} \tag{11}$$

with $\langle M^2 \rangle$ the fluctuation of the total dipole moment of the simulation box, which is implemented in the GROMACS engine[47] is initially around $g_k = 0.5$, indicating a significant correlation of dipole moments. It changes after the annealing to $g_k = 0.02$, showing that the dipole–dipole alignment is weakened considerably in the bulk.

The reduction in dipole moment was enough to eliminate the torque on the slabs which was observed to cause significant slab angular movement in preliminary trajectories using the system before annealing.

Constraint-Force Pulling and Thermodynamics of Separation. In order to validate the stability of the simulations, the densities are plotted as a function of separation in

dx.doi.org/10.1021/jp300230p | J. Phys. Chem. B 2012, 116, 5933–5940

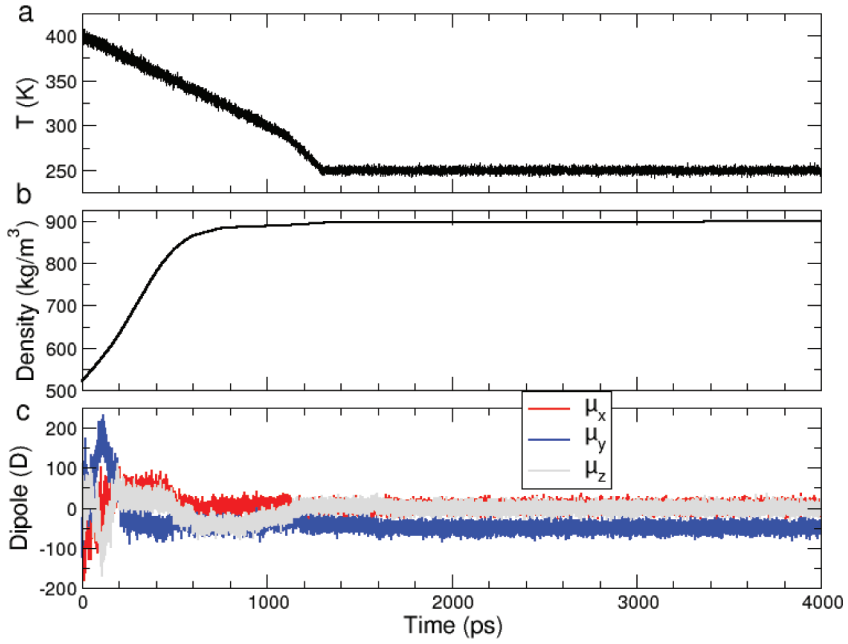

Figure 2. Simulated annealing of hydrate structure. Properties shown (a) temperature, (b) density, and (c) components of the total dipole.

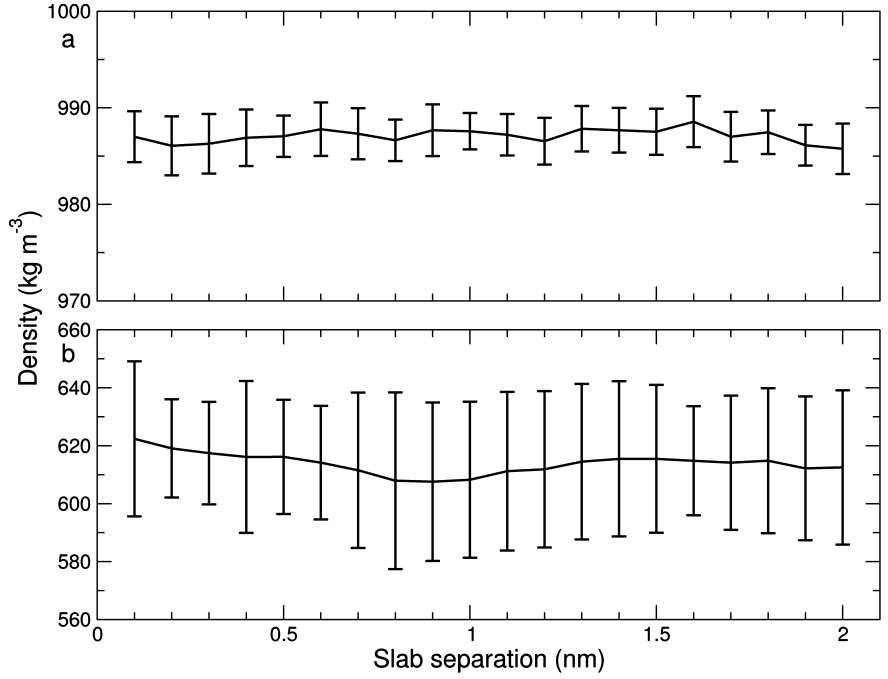

Figure 3. Density in the simulations (a) hydrate II/water and (b) hydrate II/octane.

Figure 3. The density is virtually constant for all distances and hence does not influence the PMFs.

The total adhesive forces on the pulled hydrates are shown in Figure 4 as functions of slab separation for the hydrate/vacuum, hydrate/oil, and hydrate/water systems. The force is normalized by the approximated contact area of the pulled slab with the fluid facing the reference slab. This area is for all three types of systems estimated as the product of the two appropriate box lengths in the hydrate/vacuum simulations.

The free energy changes in the separation process of hydrate slabs in the three fluids are given in Figure 5.

Representative excess thermodynamic properties using the values at the smallest sampled separation of 0.1 nm as references are shown in Figures 6 and 7.

The free energy of the separation process is positive upon separation in oil and vacuum, that is, there is a net cohesive force pulling the hydrate slabs together. In vacuum this is driven both entropically and energetically in equal measure. In oil the situation is, according to the results, more ambiguous due to the uncertainty of the internal energy determination.

The behavior of the hydrate II/water system is qualitatively different from that of the other two systems examined, as seen clearly in Figure 8. There is a very slight repulsive force

dx.doi.org/10.1021/jp300230p | J. Phys. Chem. B 2012, 116, 5933−5940

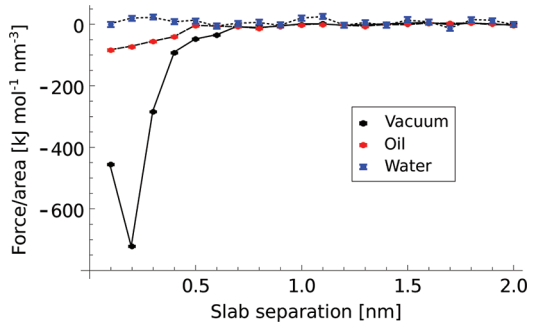

Figure 4. Normalized hydrate−hydrate adhesion force in vacuum, oil, and water.

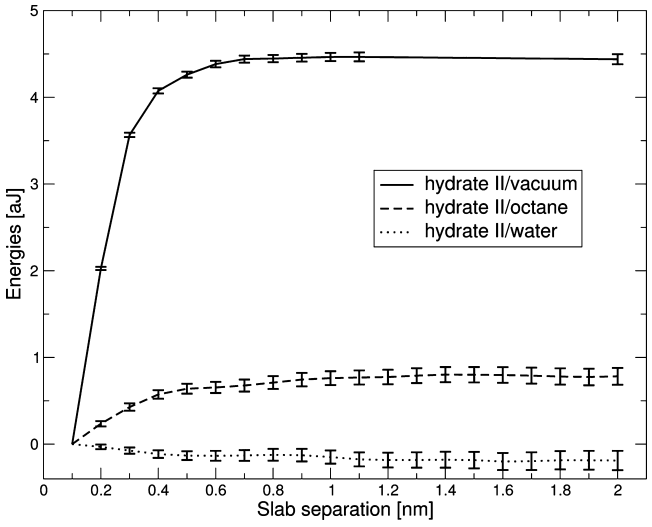

Figure 5. Free energies of separation of the three hydrate II systems.

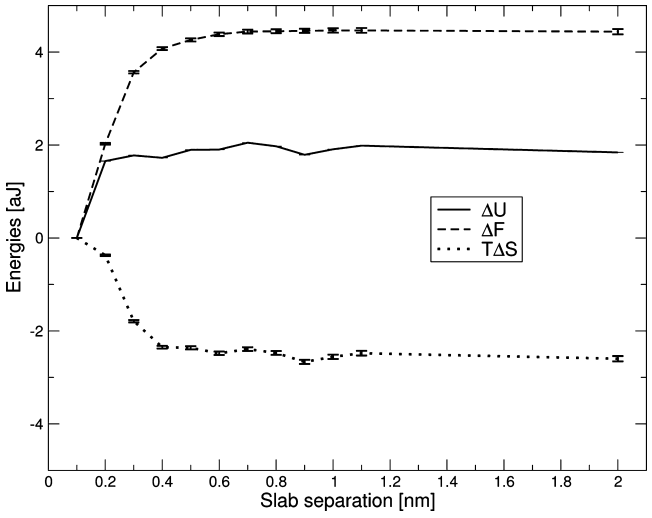

Figure 6. Thermodynamic properties for hydrate II slab separation in vacuum. Reference separation: 0.1 nm.

between the hydrate slabs, much smaller and even qualitatively different from the significant attractive forces between the slabs in the other two systems, notably also in the less polar liquid, oil.

One could speculate that a "mirroring effect" could take place due to the periodic boundary conditions in the *z*-direction. However, the system was designed to avoid such an effect with

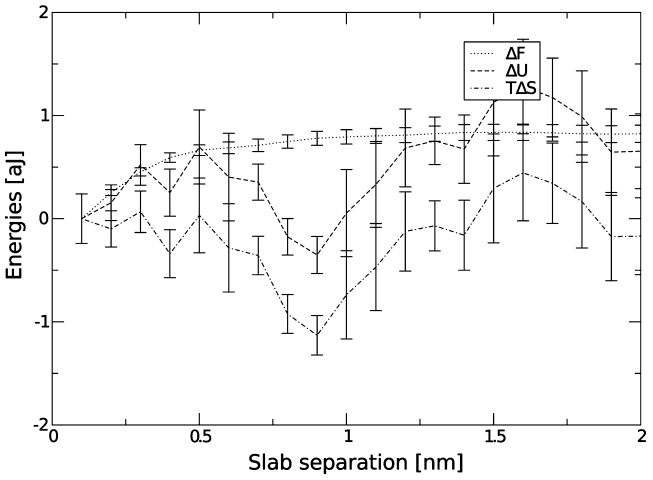

Figure 7. Thermodynamic properties for hydrate II slab separation in oil. Reference separation: 0.1 nm.

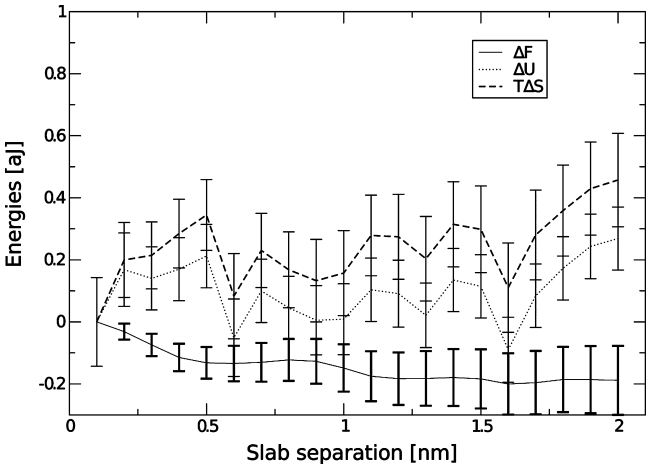

Figure 8. Thermodynamic properties for hydrate II separation in water. Reference separation: 0.1 nm.

a box length along the direction of pulling in the hydrate/fluid sims of 12 nm, of which the solid hydrate fills a length of 6.92 nm. In this system, the separation would have to exceed 2.5 nm before a mirror symmetry of the force due to the periodic boundary conditions would begin to show. Since the force goes to zero within a significantly shorter range than this, such a mirroring effect should not influence the results of the simulations.

Metrics for the convergence of the force data can be given as the deviations of the third and fourth cumulants from the normal distribution. For the hydrate−vacuum simulations the average deviation of the third and fourth cumulants from the normal distribution were 0.0108 ± 0.0346 and 0.0100 ± 0.0347, respectively, for the hydrate−oil simulations these values were 0.00077 ± 0.0539 and 0.0645 ± 0.0582, respectively, and for hydrate−water 0.0045 ± 0.0450 and 0.0276 ± 0.0436, respectively, where the uncertainties are one standard deviation. Complete tables of these values are available from the authors.

Hamaker Constants. *Theoretically Determined Hamaker Constants for Structure II in Vacuum and Oil.* In order to use (6) to calculate the Hamaker constants, the results of Bonnefoy et al.[23,48] for the dielectric properties of water and ice, together with their use of a series of Clausius−Mosotti mixing rules, assuming equal polarizabilities of water in both ice and hydrate

dx.doi.org/10.1021/jp300230p | J. Phys. Chem. B 2012, 116, 5933−5940

are applied below. However, since this work focuses on pure propane gas hydrate, slightly different results are obtained due to the change in densities and cage occupancies.

At a temperature of 253 K and a pressure of 1 bar the densities are: ice ρ_i = 917 kg/m^3; propane ρ_f = 2.1 kg/m^3; hydrate cages ρ_e = 800 kg/m^3, and guests ρ_g = 115 kg/m^3. The static dielectric constants are ice: 96.5; propane gas: 1.0022; and hydrate II: 24.3. The dielectric response function of hydrate in vacuum is plotted in Figure 9 and compared with that of structure I.[23]

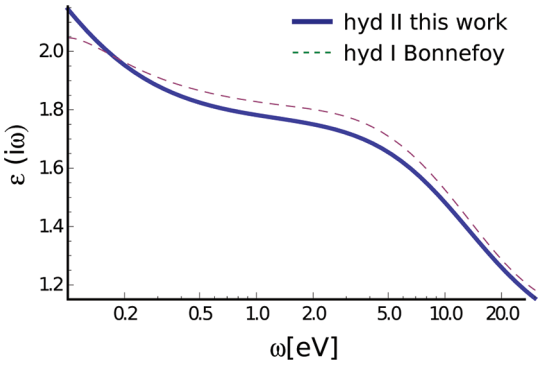

Figure 9. Dielectric response of propane hydrate calculated in this work compared with that of methane hydrate as given by Bonnefoy et al.[23]

In this work retardation effects are not corrected for, due to the small system size.

Now calculating from (6), in discrete steps of 0.14 eV in the range ω_n: [0.4, 30] eV a Hamaker constant A_{hvh} = 23 kJ/mol is obtained. This is very close to that of Bonnefoy et al. for structure I, which was 26 kJ/mol.

Dielectric data for octane are taken from Hough and White[49] using the Ninham−Parsegian two-term expansion.[50] The static dielectric constant of octane is 1.95. The Hamaker constant is then calculated to be A_{hoh} = 2 kJ/mol.

Hamaker Constants from Simulations. The fitting function is the derived force of the potential equation (5). To achieve a good fit to the data at very small separations, a repulsive r^{-9} term is, as mentioned earlier in the paper, added (see eq 3). However, this term is insignificant for all separations above 0.1 nm in each series and does not significantly alter the value of the attractive term.

In the case of the hydrate II/vacuum simulations no space is left on the external faces of the hydrate slabs in the homogeneous directions, as illustrated in Figure 1. This means that the system effectively consists of two infinite slabs, $L \to \infty$ and f reduces to

$$f_\infty = \frac{1}{12\pi D^2}$$

In the other systems the hydrate is surrounded by fluid, but the ratio D/L is never greater than 1/2. This means that for the furthest separations of $D = D_{max}$ the expression becomes

$$f \le 3f_\infty \qquad (12)$$

where D is kept fixed.

A Hamaker constant of A_{hvh} = 113 ± 4 kJ/mol is found for hydrate/vacuum/hydrate. This is approximately a factor 4 larger than the theoretical prediction.

Since the hydrate/oil system has a finite-sized slab, the Hamaker constant is found by applying the maximal geometric correction (12). The Hamaker constant in this case is found to be A_{hoh} = 4.5 ± 0.5 kJ/mol. Also, this exceeds the expected value, calculated from DLP theory above, by a factor of 2.5.[23]

The forces in the hydrate/water/hydrate case are so small that it is not possible to determine a value for the Hamaker constant in this case.

The Hamaker constants determined in this manner agree in terms of order-of-magnitude with the expectations, and also the differences between the different systems agree with what might be expected, showing that this type of simulation is viable for determining hydrate particle interaction. Deviations may be explained by a number of factors. The water models in these simulations are nonpolarizable, and this may explain a stronger interaction, since there is no shielding effect in the crystals where the water molecules are fixed. Some deviation could also be caused by the residual dipole moments, edge effects, and other size-related effects.

CONCLUSION

Quantitative estimates of the van der Waals forces between two hydrate slabs in three different environments have been made by direct molecular simulations. The forces between the simulated surfaces are found to have a range of no more than 1.5−2 nm, which may have importance for the mechanism of action of antiagglomerant molecules.

Furthermore, it is found that hydrate interacts most strongly in vacuum and progressively less so in octane and water. The interaction of hydrate in vacuum and oil is attractive, for vacuum the attraction is driven equally by entropy and energy change, and for oil the picture is less clear but the attraction is driven to a larger degree by entropy.

The interaction of hydrate in water is somewhat more complicated but is found from the simulations to be very mildly repulsive. Also, this interaction looks primarily entropically driven, although the uncertainty of this latter conclusion is large.

The values of the forces are of the same order of magnitude but higher than the predictions of DLP theory, likely due to the fact that classical Hamaker theory ignores many-body interactions and the effects of polarization.

The implications of this study is that it is possible to obtain results for the interaction between the surfaces of hydrate particles in various environments that qualitatively vary in the way expected and quantitatively are at least of the right order of magnitude. This opens up new lines of inquiry, such as (1) the effect of various oils on the particle interaction can be studied; (2) it should be possible in slightly larger systems to model the behavior of liquid water adsorbed on the hydrate surfaces in an oily environment, possible leading to bridging; and (3) various types of molecules, such as molecules to be tested for deagglomerant effects, can be added to the fluid between the surfaces to study their effect on the forces acting between the surfaces

AUTHOR INFORMATION

Corresponding Author

*E-mail: alex.hoffmann@ift.uib.no.

Notes

The authors declare no competing financial interest.

REFERENCES

(1) Sloan, E. D.; Koh, C. A. *Clathrate Hydrates of Natural Gases*, 3rd ed.; CRC Press: Boca Raton, FL, 2008; Vol. *119*.
(2) Sloan, E. D. *Fluid Phase Equilib.* **2005**, *228*−*229*, 67−74.
(3) Ballard, A. L. *Chem. Eng. Sci.* **2001**, *56*, 6883−6895 0009−2509.
(4) Makogon, Y. F.; Holditch, S. A.; Makogon, T. Y. *J. Pet. Sci. Eng.* **2007**, *56*, 14−31.
(5) Dawe, R. A.; Thomas, S. *Energy Sources, Part A* **2007**, *29*, 217−229.
(6) Hovland, M. *Energy Explor. Exploit.* **2000**, *18*, 339−347.
(7) Davies, S. R.; Selim, M. S.; Sloan, E. D.; Bollavaram, P.; Peters, D. J. *AIChE J.* **2006**, *52*, 4016−4027.
(8) Koh, C.; Westacott, R.; Zhang, W.; Hirachand, K.; Creek, J.; Soper, A. *Fluid Phase Equilib.* **2002**, *194*, 143−151.
(9) Kelland, M. A. *Energy Fuels* **2006**, *20*, 825−847.
(10) Gordienko, R.; Ohno, H.; Singh, V.; Jia, Z.; Ripmeester, J.; Walker, V. *PLoS One* **2010**, *5*, e8953.
(11) Hoiland, S.; Askvik, K. M.; Fotland, P.; Alagic, E.; Barth, T.; Fadnes, F. *J. Colloid Interface Sci.* **2005**, *287*, 217−225.
(12) Hemmingsen, P. V.; Li, X. Y.; Peytavy, J. L.; Sjoblom, J. *J. Dispersion Sci. Technol.* **2007**, *28*, 371−382.
(13) Askvik, K. M.; Hoiland, S.; Fotland, P.; Barth, T.; Gronn, T.; Fadnes, F. H. *J. Colloid Interface Sci.* **2005**, *287*, 657−663.
(14) Rusanov, A. I. *Surf. Sci. Rep.* **1996**, *23*, 173−247.
(15) Smelik, E. A.; King, H. E. *Am. Mineral.* **1997**, *82*, 88−98.
(16) Ohmura, R.; Matsuda, S.; Uchida, T.; Ebinuma, T.; Narita, H. *Cryst. Growth Des.* **2005**, *5*, 953−957.
(17) Doppenschmidt, A.; Kappl, M.; Butt, H. J. *J. Phys. Chem. B* **1998**, *102*, 7813−7819.
(18) Taylor, C.; Dieker, L.; Miller, K.; Koh, C.; E., S., Jr. *J. Colloid Interface Sci.* **2007**, *306*, 255−261.
(19) Mastny, E. A.; Miller, C. A.; de Pablo, J. J. *J. Chem. Phys.* **2008**, *129*, 034701.
(20) van der Spoel, D.; Wensink, E. J. W.; Hoffmann, A. C. *Langmuir* **2006**, *22*, 5666−5672.
(21) Israelachvili, J. N. *Intermolecular and Surface Forces*, 3rd ed.; Academic Press: London, 2011.
(22) Dzyaloshinskii, I.; Lifshitz, E.; Pitaevskii, L. *Phys.-Usp.* **1961**, *4*, 153−176.
(23) Bonnefoy, O.; Gruy, F.; Herri, J. M. *Fluid Phase Equilib.* **2005**, *231*, 176−187.
(24) Frenkel, D. D. *Understanding Molecular Simulation: From Algorithms to Applications/Daan Frenkel, Berend Smit* **2002**.
(25) Jorgensen, W. L.; Maxwell, D. S.; Tirado-Rives, J. *J. Am. Chem. Soc.* **1996**, *118*, 11225−11236.
(26) Abascal, J. L. F.; Sanz, E.; Fernandez, R. G.; Vega, C. *J. Chem. Phys.* **2005**, *122*, 234511.
(27) Miyamoto, S.; Kollmann, P. *J. Comput. Chem.* **1992**, *13*, 952−962.
(28) Hess, B. *J. Chem. Theory Comput.* **2008**, *4*, 116−122.
(29) Thompson, M. A. ArgusLab 4.0.1. Planaria Software LLC, Seattle, WA.
(30) Schuttelkopf, A. W.; van Aalten, D. M. F. *Acta Crystallogr., Sect. D* **2004**, *60*, 1355−1363.
(31) van der Spoel, D.; Lindahl, E.; Hess, B.; Groenhof, G.; Mark, A. E.; Berendsen, H. J. C. *J. Comput. Chem.* **2005**, *26*, 1701−1718.
(32) Humphrey, W.; Dalke, A.; Schulten, K. *J. Mol. Graphics* **1996**, *14*, 33.
(33) Kaminski, G. A.; Friesner, R. A.; Tirado-Rives, J.; Jorgensen, W. L. *J. Phys. Chem. B* **2001**, *105*, 6474−6487.
(34) Jorgensen, W. L. *J. Chem. Phys.* **1983**, *79*, 926−935.
(35) McMullan, R. K.; Jeffrey, G. A. *J. Chem. Phys.* **1965**, *42*, 2725−2732.
(36) Chazallon, B. *J. Chem. Phys.* **2002**, *117*, 308−320.
(37) Hess, B.; Kutzner, C.; van der Spoel, D.; Lindahl, E. *J. Chem. Theory Comput.* **2008**, *4*, 435−447.
(38) van der Spoel, D.; Lindahl, E.; Hess, B.; van Buuren, A. R.; Apol, E.; Meulenhoff, P. J.; Tieleman, D. P.; Sijbers, A. L. T. M.; Feenstra, K. A.; van Drunen, R.; Berendsen, H. J. C. GROMACS User Manual version 3.3, 2005.
(39) Essmann, U. *J. Chem. Phys.* **1995**, *103*, 8577−8593 , 0021−9606.
(40) Berendsen, H.; Postma, J.; van Gunsteren, W.; Dinola, A.; Haak, J. *J. Chem. Phys.* **1984**, *81*, 3684−3690.
(41) Ryckaert, J.-P.; Ciccotti, G.; Berendsen, H. J. C. *J. Comput. Phys.* **1977**, *23*, 327−341.
(42) Bernal, J. D.; Fowler, R. H. *J. Chem. Phys.* **1933**, *1*, 515−548.
(43) Tanaka, H. *J. Chem. Phys.* **1994**, *101*, 10833−10842.
(44) Pan, D.; Liu, L. M.; Tribello, G. A.; Slater, B.; Michaelides, A.; Wang, E. *Phys. Rev. Lett.* **2008**, *101*, xxxx.
(45) Suman, B.; Kumar, P. *J. Oper. Res. Soc.* **2006**, *57*, 1143−1160.
(46) Kirkwood, J. G. *J. Chem. Phys.* **1939**, *7*, 911−919.
(47) Nymand, T. M.; Linse, P. *J. Chem. Phys.* **2000**, *112*, 6386.
(48) Bonnefoy, O.; Gruy, F.; Herri, J. *Mater. Chem. Phys.* **2005**, *89*, 336−344.
(49) Hough, D. B.; White, L. R. *Adv. Colloid Interface Sci.* **1980**, *14*, 3−41.
(50) Ninham, B. W.; Parsegian, V. A. *Biophys. J.* **1970**, *10*, 646.